Visualisation of fresh cut timber deformation by photogrammetry

Eve Walkden Ph.D.

Senior Technician

Department of Architecture & Civil Engineering

University of Bath

Claverton Down

Bath BA2 7AY

United Kingdom

Alan Bloodworth Ph.D. C.Eng

Principal Teaching Fellow

School of Engineering

University of Warwick

Library Road

Coventry CV4 7AL

United Kingdom

Abstract

Understanding the mechanical behaviour of fresh cut timber, in which the natural moisture content has been retained, has application in predicting the behaviour of living tree elements such as branch/stem joints, potentially inspiring structural designs through biomimicry. This project develops a process of strain imaging using particle image velocimetry to analyse behaviour of timber samples freshly cut from oak tree joints and tested in tension. The timber surface was not coated so the fibre response could be visualised directly. Load was applied in steps, and different methods for comparing images trialled, including a sequential method in which strain is accumulated progressively from image to image, and a first-to-last comparison. Sample flexibility caused significant deformation in the camera field of view, and so the analysis methodology was modified so that each image was compared sequentially with the first with the target area in the image for strain calculation expanded as the test proceeded. This resulted in strain contour plots able to show the impending failure of the component as the tension is applied.

Keywords: Timber, photogrammetry, structural testing

Introduction

The behaviour and specifically the strain distribution in fresh cut timber under load is complicated by the fibrous nature of the material and by local moisture changes as it is loaded. Electrical strain gauges cannot detect strains in individual fibres and their attachment may be compromised by surface moisture or loose fibres. Strain calculated from machine stroke, *i.e*. relative displacement of the end grips, is affected by slip of the sample and local tearing of the fibres under the grips.

Photogrammetry applies an algorithm of image recognition to compare two digital images taken before and after the movement of a target area to give the full-field deformation of the sample. Previous experience of its use on timber include Choi *et al.* (1991) who analysed video taken of painted wood/paper samples under load with a microscope. Franke *et al.* (2007) used timber coated with white wax film, with the addition of specific measurement points, although this does not provide as clear a picture of timber fibre behaviour as observing the actual timber surface. Thus both Franke *et al.* (2007) and Choi *et al.* (1991) applied a film coating and monitored specific target points; however, this does not exploit the whole benefit of full-field photogrammetry.

Godara *et al.* (2009) used digital image correlation (DIC) to observe structural integrity of a composite material reinforced by natural wood fibres. Localised strains within the composite material were qualitatively analysed and mapped. Particle image velocimetry (PIV) was first used in fluid mechanics to measure flow velocity by seeding a flow with mica particles, taking two consecutive exposures on one light sheet or traditional film, and then constructing an image intensity field inside a series of interrogation volumes. A correlation could then trace and record the maximum movement of the interrogation volumes (Raffel *et al*. 2007). As such, the technique is not limited to just tracking the movement of discrete targets.

With modern digital technology and software, PIV has gained higher efficiency and reliability and many different implementations exist for varying applications. Digital PIV using a single camera has been used to measure the displacement field in soil (White *et al.* 2003) and of plant roots (Hamza *et al.* 2006). In this research, a code to implement PIV developed by White and Take (2002) was adapted for sequential analysis of images of timber samples tensile load. Its effectiveness in detecting pre-failure strain response and early signs of sample failure is assessed.

The PIV method

Digital images are taken of the subject at two different loading steps. Within both images, a *target area* (for example, the front surface of the sample) is defined, and in the first image sub-divided into *interrogation areas* (IA) (Fig. 1). The objective is to obtain the displacement of the centre of each IA in the second image. This is done by defining in the second image a *search area* (SA) for each IA in the first image and searching within this area for the best location of the IA from the first image. This best location is obtained using a statistical correlation method by which the tricolour value (red, green and blue, each ranging between 0 to 255) in each pixel in the IA in the first image is compared with the corresponding pixel in every possible IA of the same size occurring in a search area in the second image (White *et al*. 2003). The location of the IA in the second image with the highest correlation coefficients for each tricolour value is used to calculate its displacement. Displacement vectors to more accurate sub-pixel level are obtained by interpolating displacement vectors with peak and sub-peak correlation coefficients. Repeating the process for every IA in the target area in the first image gives the approximately the full-field displacement field, which can be differentiated to obtain full-field strains.

The implementation of the PIV analysis in the program by White and Take (2002) uses normalized cross-correlation and two-dimensional spatial Hermite bicubic surface interpolation to obtain the displacement vector to sub-pixel accuracy (White *et al*. 2005).

Strain calculation

The small strain assumption was considered appropriate for timber under load. Horizontal and vertical direct strains (ε_x, ε_y), and shear strains (τ_{xy}) are as follows:

$$\varepsilon_x = \frac{\Delta u}{\Delta x} \qquad (1a)$$

$$\varepsilon_y = \frac{\Delta v}{\Delta y} \qquad (1b)$$

$$\gamma_{xy} = \gamma_{yx} = \frac{\Delta u}{\Delta y} + \frac{\Delta v}{\Delta x} \qquad (1c)$$

Where Δu and Δv are the difference in horizontal and vertical displacements between IAs with horizontal and vertical spacings Δx and Δy respectively, the base lengths for strain calculation.

As an alternative, true strain can be calculated to reflect the incremental deformation of the material. As an example in the vertical direction:

$$(\varepsilon_x)_{true} = \ln\left(\frac{\Delta u}{\Delta x}\right) \qquad (2)$$

The relationship between true strain and engineering strain is as follows:

$$(\varepsilon_x)_{true} = \ln(1+\varepsilon_x) \qquad (3)$$

Application of PIV to timber component testing

Sample preparation and test setup

Figure 2 shows the test setup in which the PIV was applied. Test samples were oak timber battens, of 25 mm square cross-section and 225 mm length between grips, loaded either in tension or compression in a Denison Mayes servo-hydraulic test machine (the two alternative positions of the sample are shown in Figure 2(a)). Samples originated in branch-stem joints selected from *Quercus Robur (L.)* oak trees harvested in the New Forest, UK in November 2010 (Walkden 2014; 2016). Once the branch joints had been cut from the trees, the angle at which the secondary growth connects to the main stem was brought through into the main stem to provide the secondary cut (Fig. 3). The sample was then further cut into linear battens (Fig. 3), which were then wrapped in film to minimise moisture loss. The time from cutting the joint samples into battens until testing was minimised as far as practicable and all tests completed within two weeks of batten cutting, with the aim of obtaining as close as possible the mechanical properties of the living tree wood. Three joints were acquired, from which a total of twenty battens were cut and tested.

A typical image from the camera viewing the front face of the sample is shown in Figure 2(b). The larger shaded area is the target area or ‘Active Area’ and the smaller shaded area is a ‘Fixed Point’ which is assumed to remain steady during the test, to allow for correction of minor camera movement.

Initial PIV trials

An initial trial of the PIV process used a basic 7.1 megapixel camera set up parallel to the front surface of sample B1 tested in tension. Photos were taken at regular intervals during a tension experiment (total of 40 images taken). The sample was painted to provide a textured surface so that tracking movements would be easier. A Graphical User Interface modified from one used by White (2002) was used to input target and search areas for a PIV analysis.

After the experiment, pairs of photos were numerically analysed using the White and Take code, by two methods. The first method compared only the last image just prior to sample failure with the first one to obtain the overall strain. The second compared each image in the test sequentially with the previous one, accumulating the strain. An aggregated ε_y for the sample calculated as a mean of the values of each IA is compared with the machine measured strain, obtained from the relative vertical displacements of the machine grips divided by the length between them.

Two problems emerged during this trial. The first was changes in lighting between images, which affected the apparent coloration of the sample. A less obvious issue is that the image was stored as a .jpeg file, which may have been too compressed for accurate pixel data analysis.

Figure 4 shows that qualitatively, the sequential analysis gave better results than the first/last image comparison, with the zone of breakage (red colour) evident to a certain extent in the ε_x and τ_{xy} strain plots, although with a lot of 'noise'. Both methods substantially over-estimated the accumulated strain compared to the machine measured value of 0.024 με (Table 1).

In the second test, on sample B2 in compression, image quality was increased with a Canon Powershot G10 (14.6 megapixel) camera, with a continuous lighting rig used to minimise lighting variations. The sample was not painted this time as it was deemed

that the fibrous quality of the regular timber would provide the texture required to analyse the image, once the lighting quality had been improved (Fig. 5).

The compression test had the disadvantage that failure (by crushing) was localised at the top so that the zone of high strain measurement was small and incomplete. The resulting bending that occurred was reflected in the ε_y contours (Fig. 6) that show tension on the right and compression on the left. The .jpeg and .tif images give slightly different contours. Table 2 shows the strain obtained from the .tif image is marginally closer to the machine measured value of $0.047\mu\varepsilon$, and hence .tif images were deemed more accurate for future comparisons.

Sequential analysis of the images would be expected to give the most accurate strain results as it compares all images over time, cumulating the strain. However, neither method gave satisfactory actual values of strain. No further obvious improvements could be made to the physical experiment setup, and so attention turned to improving the analysis code.

Code development

The graphical user interface (GUI) modified from that used by White and Take (2002) had the disadvantages that only a pair of images could be analysed at once and selection of the target areas was a manual process that lacked repeatability between images. Therefore, a new GUI was developed in Matlab® with the following features:

- An initial input screen (Fig. 7) on which the target grid was specified and then tracked throughout all subsequent images.
- The ability to analyse a number of images automatically and combine results efficiently to display development of strain with ‘time’ through the analysis.

Movement of the camera needed to be tracked to ensure that the Active Area remained accurately positioned relative to the sample. This meant the Fixed Point needed to be tracked throughout multiple images.

There were two options for tracking the Active Area once correction for camera movement had been applied (Fig. 8):

1. Select one Active Area in the first photo and use it throughout all subsequent photos.
2. Track the change in position of the Active Area in each sequential photo, updating it each time.

The problem with the first option is that it is likely that since the fibres change in appearance slightly as each increment of load is applied, the IA's colouration eventually change too much to be accurately tracked. The second option should be better able to determine the strain but meant creating a code that tracked the movement of the Active Area.

The same tracking options are available for correcting for camera movements using the Fixed Point. However, since the Fixed Point is not subject to any strain or change in texture, it is sufficient to track all camera movements relative to the Fixed Point in the original image, as in option 1 above.

Interrogation Area size

The size (in pixels) of each element of the Active Area grid affects the accuracy of PIV results. The smaller the IA size, the higher spatial resolution of strain data obtained, but the increased likelihood of error in tracking individual squares. A study was done using sample G1S with 10x10, 20x20 and 30x30 pixel IAs on a first-last comparison, and the

20x20 element size found to give the most plausible contour plot and therefore selected for subsequent use, although element sizes were reviewed when necessary.

Trial analysis with new GUI

Having decided the calculation and tracking techniques and grid element sizes, the code was run on sequential images taken of the side view of sample G1 ('G1S', Fig. 7). The results (Fig. 9) show some prior evidence in all three strain components of the breakage occurring just below mid-height. ε_y is largest as expected, but ε_x also indicates the failure. Larger strains both in tension and compression are also noted towards the top of the plots, caused by localised pinching of the grips against the sample. Average ε_y from PIV calculated to be 0.095με, lower than the machine strain of 0.12με, although this is expected if there is some slip of the sample in the grips during the test.

The indication was that the methodology worked in principle, however there was a need to refine it so failure areas were visually easier to comprehend.

Additional fixed points to track Active Area

Before and after images of the G1S sample (Fig. 10) highlight how the sample not only stretched but moved upwards relative to the analysis target area. Figure 11 shows that a Fixed Point located on the bottom grip of the machine also experiences vertical upward movement as the load is increased and the grips embed onto the sample and slide upward in the tapered blocks. It was clear that both these movements needed to be taken into account to improve the accuracy of the PIV analysis.

A total of five Fixed Points were therefore defined (Fig. 12). The original rigid Fixed Point (RFP) adjusts for x-direction movements of the camera, by comparing with its position in the initial image (Figure 8, option 1). The Fixed Point of the bottom grip

(BGFP) tracks the *y*-position of the bottom of the Active Area, cumulating between images (Figure 8, option 2). The *y*-position of the Fixed Point of the top grip (TGFP) minus that of the BGFP determines the change in length of the sample over the Active Area. However, the Active Area itself would be increased in length only if its stretch accumulated to the size of the PIV grid, so that another row of data could be added (Fig. 13).

The other two points tracked are on the sample itself, in the top (TSFP) and bottom (BSFP) slip zones. From these it was hoped to determine the slip of the sample ends relative to the grips, so as to obtain a more direct measure of overall sample *y*-direction strain than averaging the strains from PIV.

Once the Active Area has been tracked in this way in a sequential analysis, a final 'last ditch' measure of sample strain can be obtained by comparing the first image with the image immediately prior to failure, using the updated Active Area. Figure 14 and Figure 15 show the detail of the tracking of the Active Area at the top and bottom of the sample respectively. In both Figures, row (i) shows the original image, and row (ii) the final image prior to failure. Column (a) shows the original Fixed Point and Active Area positions and column (b) the new positions as a result of the tracking. The benefit of the tracking can be seen by comparing the top left and bottom right images in each Figure. It can be seen how the grip Fixed Points (TGFP, BGFP) provided a clearer indication of movement compared to the Fixed Points on the sample (TSFP, BSFP) where the tracking could be mistaken through the close texture of the surface. Therefore the track of the grips was used in the coding to move and stretch the Active Area zone. Comparison of the top right and bottom left images in Figure 15 shows how the upward movement of the machine grips affected the tracked Active Area, which contributed to the previous inaccuracies but was now accounted for in the PIV code.

Comparison between sequential and first-last methodologies with Active Area tracking

The images of sample G1S from the start of the test to the last image before failure were re-analysed in two ways with Active Area tracking; firstly by the sequential method and secondly with a first-to-last comparison.

In the sequential results (Fig. 16) increasing strains appear as dark areas at the top and at about a third from the bottom of the sample. Strains are registered in all three directions, suggesting a diagonal failure will occur. Strains at the top are likely to be due to the progressively increasing grip on the sample. The zone a third from the bottom is the focus of the potential breakage.

On closer inspection of Figure 16, the zone of strain concentration is not the actual point of failure but where grain rings were found. Following the rings around, the breakage occurred where the spacing between the grain rings narrows (a point where medullary rays were confined together).

The first-last comparison shows the failure of the sample and style of break as dark areas of strain on Figure 17, highlighted by the dotted line just below. Average strains from the two methodologies are both much closer to the machine measured strain of 0.12με (Table 3).

The sequential analysis with Active Area tracking gave improved results compared to the original first-last method. Further improvement was sought through a first-sequential analysis, in which the first image is compared to each subsequent image, expanding and tracking the search zone as described above. Figure 18 and Figure 19 show the potential for improved strain visualisation by this method.

The final overall strain of 0.105με from the first-sequential analysis compares well with the machine value of 0.12με, as does the development of strain through the test (Fig. 20).

Evaluation

The first-sequential analysis shows promise as the most accurate calculation method for full-field strain on timber. Results presented here have been for sample G1S with 10x10 pixel IA size. This has reduced instances of double matching of IA displacements compared to 20x20 pixel IA size, but with four times the processing time. Double matching occurs when two different IA displacements in the search area correlate equally well with the original image, and the response of the program is to take the average of the two displacements. This will cause a small error in the strain field locally, although neighbouring IAs are not normally affected and therefore the extent of the error is usually limited.

The remaining samples were solved with 20x20 pixel IA size and averaging of double matches. Their detailed results of applied load with time, stress against strain, failure mode and PIV strains from sequential, and first-last and first-sequential analysis are shown in Figures S1-S323 in the Supplemental data accompanying this paper. Of the 20 specimens tested, four failed either in or very close to the bottom grip, so that the failure zone could not be detected by the PIV. Results for the other samples show the first-sequential analysis performing much better than the other methodologies in providing prior evidence of impending failure in the strain plots, with it able to do so in ten out of 16 samples and with slight evidence of doing so in a further four samples (Table S1 in the Supplemental data).

Summary and conclusions

Obtaining full-field visualisation of strains by photogrammetry for fresh cut timber samples tested in tension or compression presents challenges due to significant deformation and movement of the sample in the test machine, exacerbated by the sample's high deformability due to its high water content, and the difficulty gripping it securely at the ends. In the simplest analysis procedure in which images are compared either sequentially or with the first image but with a fixed target area selected in the first image, results proved to be inaccurate, with only vague prior visibility of failure in strain contour plots. Improvements to the analysis were therefore made with inclusion of more reference points, enabling movement and stretching of the target area to be tracked in progressive images. Accompanying this, the user interface was developed to automatically import and compare large numbers of successive images.

However, a sequential analysis in which strains are aggregated image by image still led to accumulation of errors, even with target area tracking. In the alternative first-last analysis, first and final images are compared directly, once an appropriate final search area had been deduced from a sequential analysis. This gave better qualitative and quantitative strain results, even showing the potential breakage point as the tension was increased.

The most promising results were obtained from first-sequential analysis, in which each image is compared in turn with the first one but allowing for tracking of changes to the target area, as for the sequential analysis. These contour plots show the clearest prior indication of failure and closest agreement of overall strain to the machine measured result.

It is however the most computationally demanding method, which may place a lower limit on grid size possible. This leads to increased occurrence of double matching of

grid displacements. Although this didn't have a significantly detrimental effect on the results in this project, if it was believed to be problem then the analysis code could be further enhanced by for example estimating which match to use by extrapolating from previous movements of the grid element in question.

Practical lessons learnt were that the timber had sufficient visual texture not to require coating, consistent lighting and a high resolution camera are needed, and using .tiff image files marginally improves accuracy.

Acknowledgements

The first author was supported in her research at the University of Southampton by ESPRC under doctoral training grant funding (Grant no. EP/P504740/1). Particular thanks are due to the Forestry Commission for donating fresh cut tree samples, and to Dr Anthony Lock of the University of Southampton for his advice in developing the program code.

Supplemental data

Table S1, Figures S1–S324 and accompanying explanatory text are available online along with a flowchart of the PIV analysis software in the ASCE Library (ascelibrary.org).

References

Choi, C., Thorpe, J. L. and Hanna, R. B. (1991). "Image Analysis to Measure Strain in Wood and Paper." *Wood Science and Technology,* 25, 251-262.

Franke, S., Franke, B. & Rautenstrauch, K. (2007). "Strain Analysis of Wood Components by Close Range Photogrammetry." *Materials and Structures,* 40, 37-46.

Godara, A., Raabe, D., Bergmann, I., Putz, R. and Muller, U. (2009). "Influence of Additives on Global Mechanical Behavior and Microscopic Strain Localization in Wood Reinforced Polypropylene Composites During Tensile Deformation Investigated Using Digital Image Correlation." *Composites Science and Tecnology,* 69, 139-146.

Hamza, O., Bengough, A., Bransby, M., Davies, M. and Hallet, P. (2006). "Biomechanics of Plant Roots: Estimating Localised Deformation with Particle Image Velocimetry." *Biosystems Engineering,* 94, 119-132.

Raffel, M., Willert, C., Wereley, S. and Kompenhams, J. (2007). *Particle Image Velocimetry - a Practical Guide Second Edition*, Springer-Verlag, Berlin.

Walkden, E.A. (2014). "Investigation into Image Technology of Timber for the Assessment of Structural Performance of Fresh-Cut Oak Tree Joints (*Quercus Robur L.*)." *PhD Thesis, University of Southampton, United Kingdom.*

Walkden, E.A. (2016). "Modelling the Strength of the Branch Attachments", *Arboricultural Journal* (accepted for publication).

White, D. J. (2002). "An investigation into the behaviour of pressed-in piles." *PhD Thesis, University of Cambridge, United Kingdom.*

White, D. J., Randolph, M., and Thompson, B. (2005). "An image-based deformation measurement system for the geotechnical centrifuge." *International Journal of Physical Modelling in Geotechnics*, 3, 1-12.

White, D. J. and Take, W. A. (2002). *GeoPIV: Particle Image Velocimetry (PIV) software for use in geotechnical testing, CUED/D-SOILS/TR322*, Department of Engineering, University of Cambridge, United Kingdom.

White, D. J., Take, W. A. and Bolton, M. D. (2003). "Soil Deformation Measurement Using Particle Image Velocimetry (PIV) and Photogrammetry." *Geotechnique*, 53, 619-631

List of Figure captions

Fig. 1. PIV principles: target area, IA array and search area in second image

Fig. 2. (a) Test setup; (b) Typical tension test sample showing 'Active Area' and 'Fixed Point' for PIV analysis

Fig. 3. (a) Branch selection cut from joint, (b) 100mm branch cross-section batten cut arrangement and (c) 150mm branch cross-section batten cut arrangement

Fig. 4. Contour plots of ε_x, ε_y and τ_{xy} from (a) sequential and (b) first-last image analyses for sample B1 (all strains in microstrain)

Fig. 5. Compression test of sample B2, (a) before failure and (b) after failure, showing compression failure at top left of sample

Fig. 6. ε_y from Sample B2 sequential analysis with (a) .jpeg and (b) .tif image files

Fig. 7. New GUI for input of PIV analysis parameters

Fig. 8. Options for tracking the Active Area through many images of an experiment

Fig. 9. (a) Failure of Sample G1S. Contour plots from sequential analysis: (b) ε_y, (c) ε_x and (d) τ_{xy}

Fig. 10. (a) 'Before' and (b) 'After' images of Sample G1S, with Active Area outlined

Fig. 11. Movements of Fixed Point on bottom grips for Sample G1F, indicated by solid lines, (a) 'Before' and dashed lines (b) 'After'

Fig. 12. Tracking Fixed Points and Active Area of sample G1S from (a) start of test to (b) pre-failure load

Fig. 13. Active Area grid expansion in response to sample stretch

Fig. 14. Fixed Points TGFP and TSFP (squares from left to right); (a) original points, first image; (b) tracked points, first image; (c) original points, final image; (d) tracked points, final image, Sample G1S

Fig. 15. Fixed Points BGFP and BSFP (squares from left to right); (a) original points, first image; (b) tracked points, first image; (c) original points, final image; (d) tracked points, final image, Sample G1S

Fig. 16. Sample G1S strains from sequential analysis including Active Area tracking: (a) ε_x, (b) ε_y and (c) τ_{xy}, with grain sketches of original and failed sample

Fig. 17. Strain ε_y for Sample G1S first-last analysis (including Active Area tracking) overlaid on failure image

Fig. 18. True strains $(\tau_{xy})_{true}$ from first-sequential analysis of Sample G1S, overlaid on failure image

Fig. 19. Sample G1S first-sequential analysis strains: (a) ε_x, (b) ε_y and (c) τ_{xy}

Fig. 20. Sample G1S strain ε_y against time for different PIV analysis methodologies including Active Area tracking, compared with machine measured

Tables

Table 1. PIV strain results compared with machine strain for Sample B1

Analysis type	Strain (με)
PIV Sequential analysis	0.2785
PIV First-last image comparison	0.0516
Machine measured	0.0240

Table 2. .tif and .jpeg strain results compared for sequential and first-last analysis of Sample B2

Image type	Sequential analysis ($\mu\varepsilon$)	First-last analysis ($\mu\varepsilon$)
.jpeg	1.4438	0.0617
.tif	1.4387	0.0613

Table 3. Comparison of PIV and machine measured strain values for Sample G1S

Strain	Value
Machine Measured	0.120 με
PIV sequential	0.212 με
PIV first-last	0.105 με

Figures

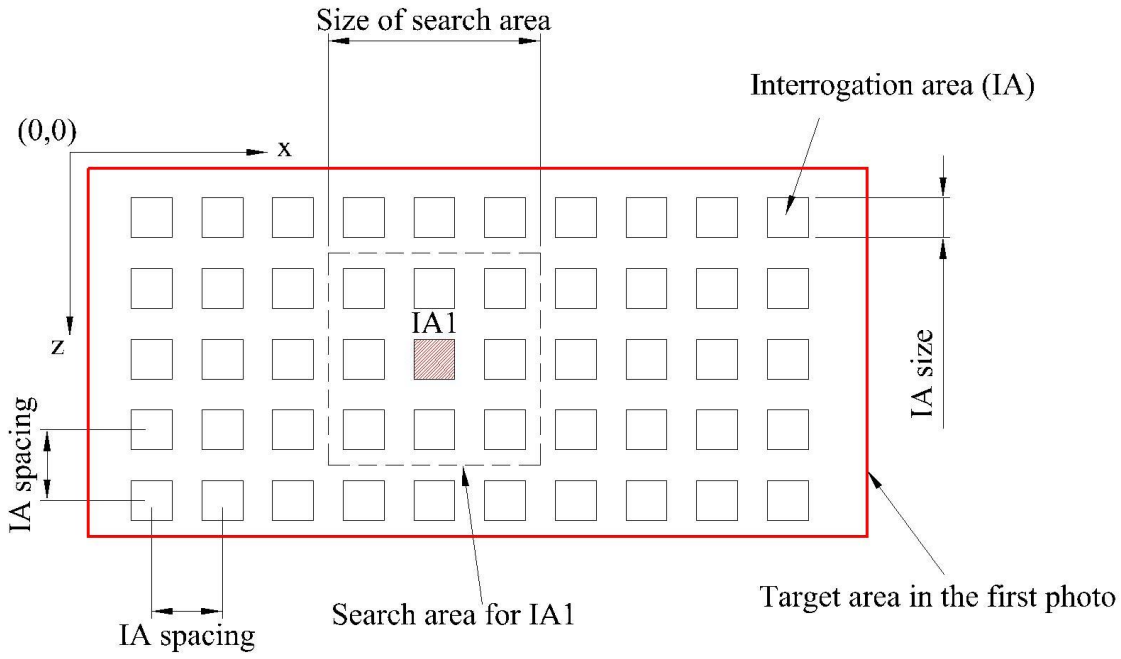

Fig. 1. PIV principles: target area, IA array and search area in second image

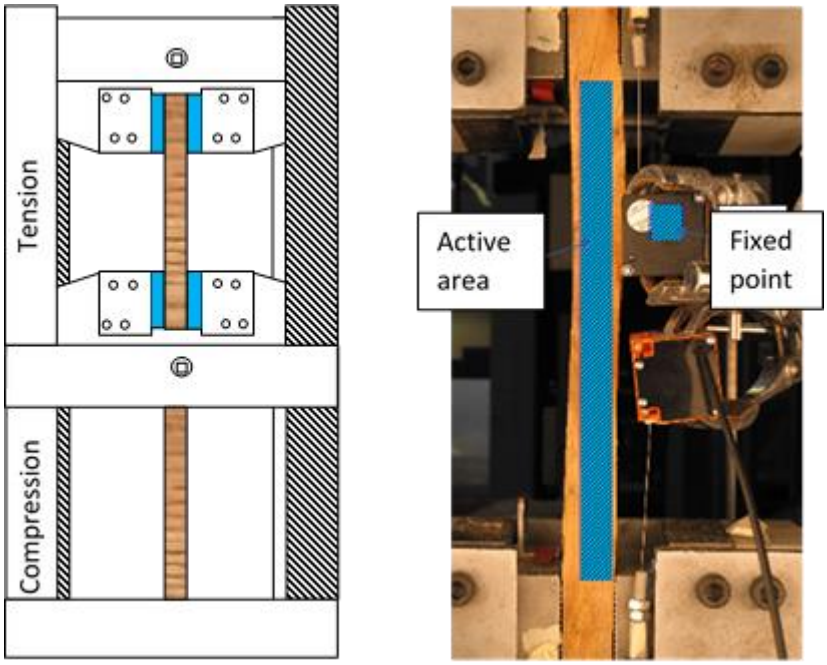

Fig. 2. (a) Test setup; (b) Typical tension test sample showing ‘Active Area’ and ‘Fixed Point’ for PIV analysis

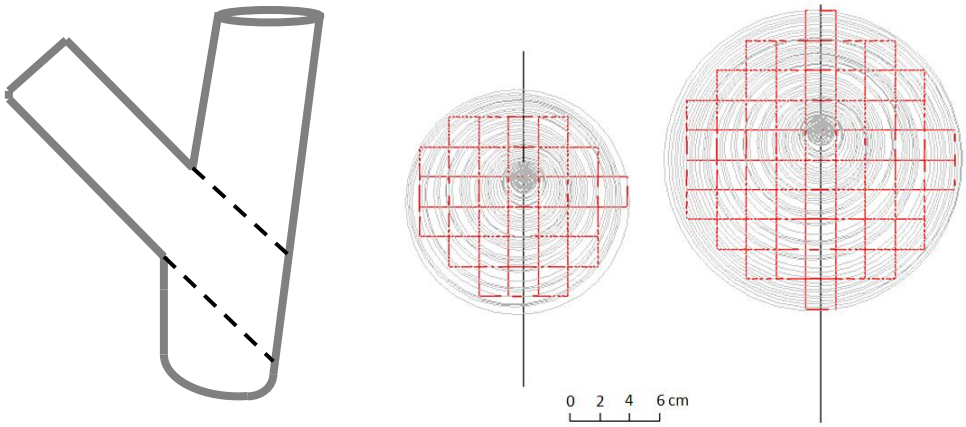

(a) (b) (c)

Fig. 3. (a) Branch selection cut from joint, (b) 100mm branch cross-section batten cut arrangement and (c) 150mm branch cross-section batten cut arrangement

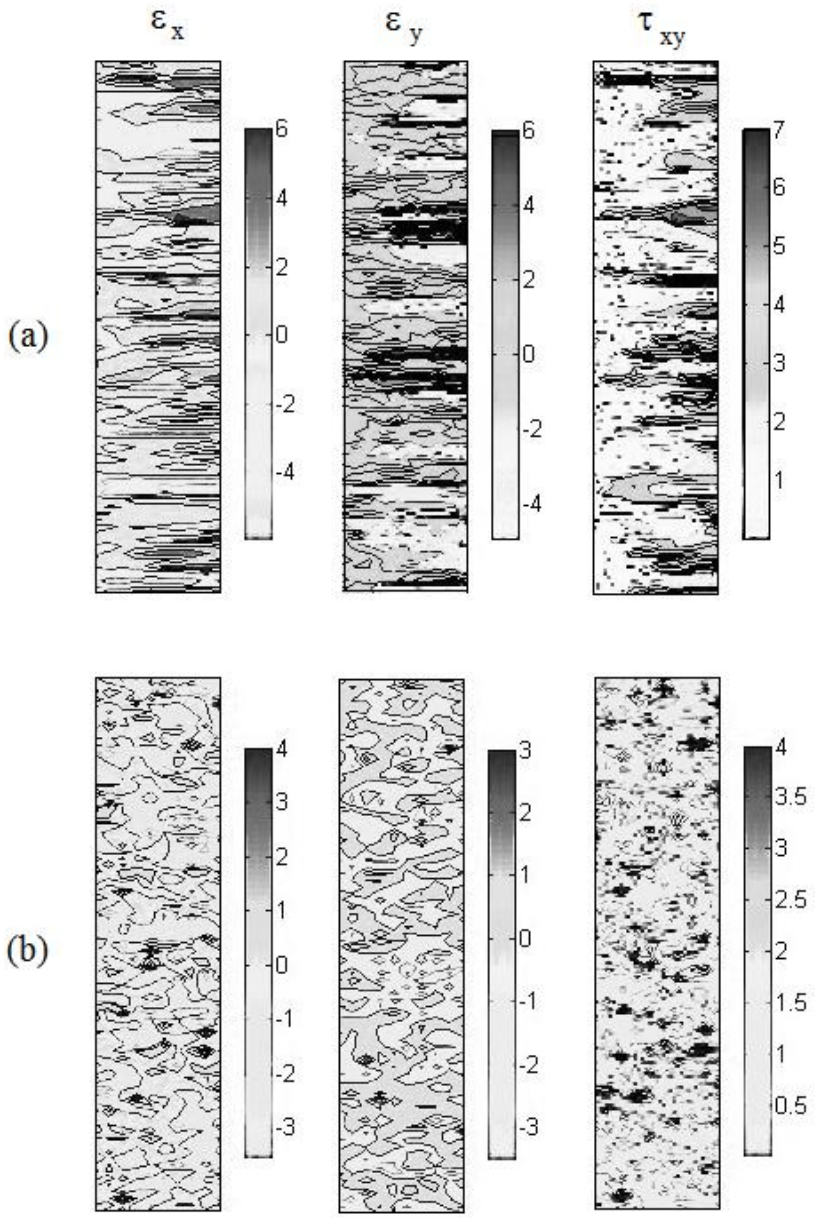

Fig. 4. Contour plots of ε_x, ε_y and τ_{xy} from (a) sequential and (b) first-last image analyses for sample B1 (all strains in microstrain)

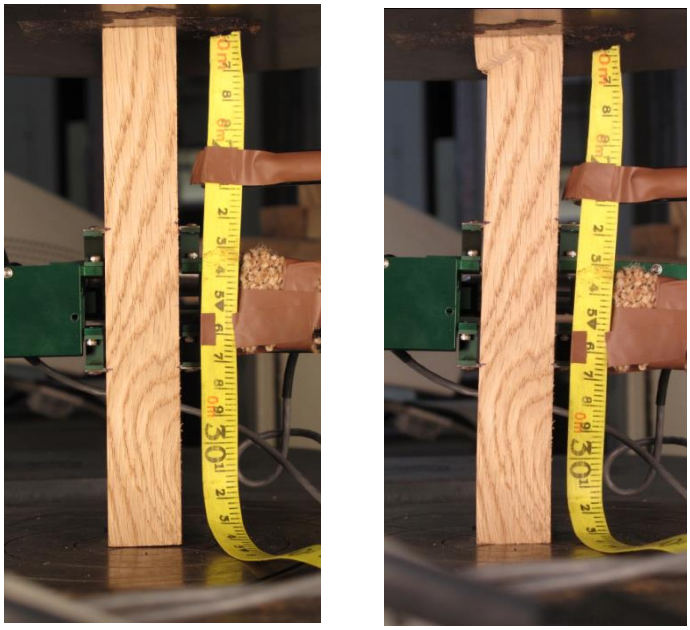

(a) (b)

Fig. 5. Compression test of sample B2, (a) before failure and (b) after failure, showing compression failure at top left of sample

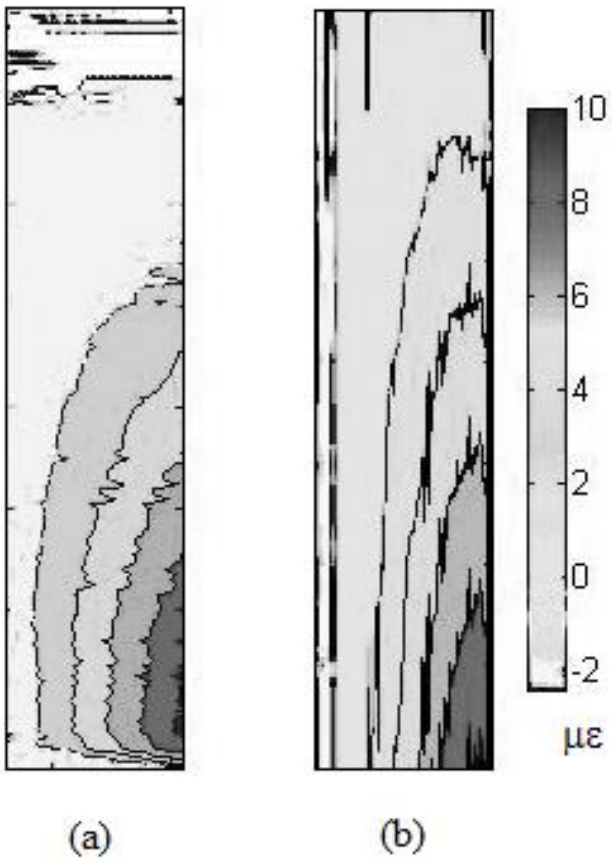

Fig. 6. ε_y from Sample B2 sequential analysis with (a) .jpeg and (b) .tif image files

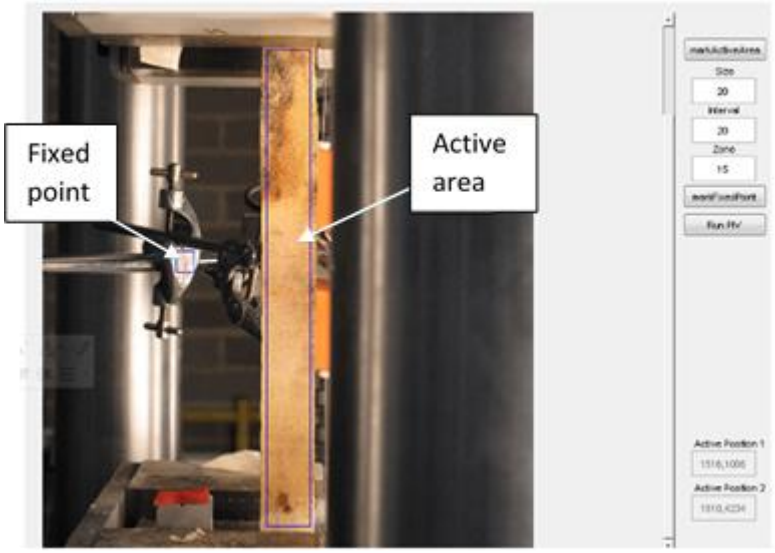

Fig. 7. New GUI for input of PIV analysis parameters

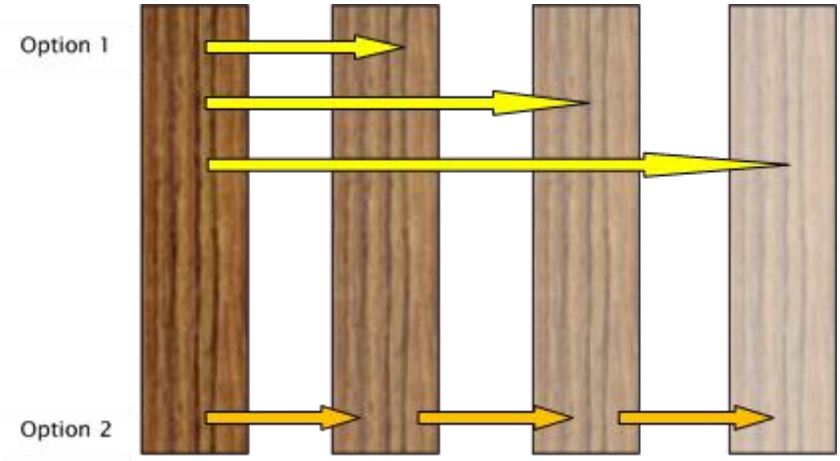

Fig. 8. Options for tracking the Active Area through many images of an experiment

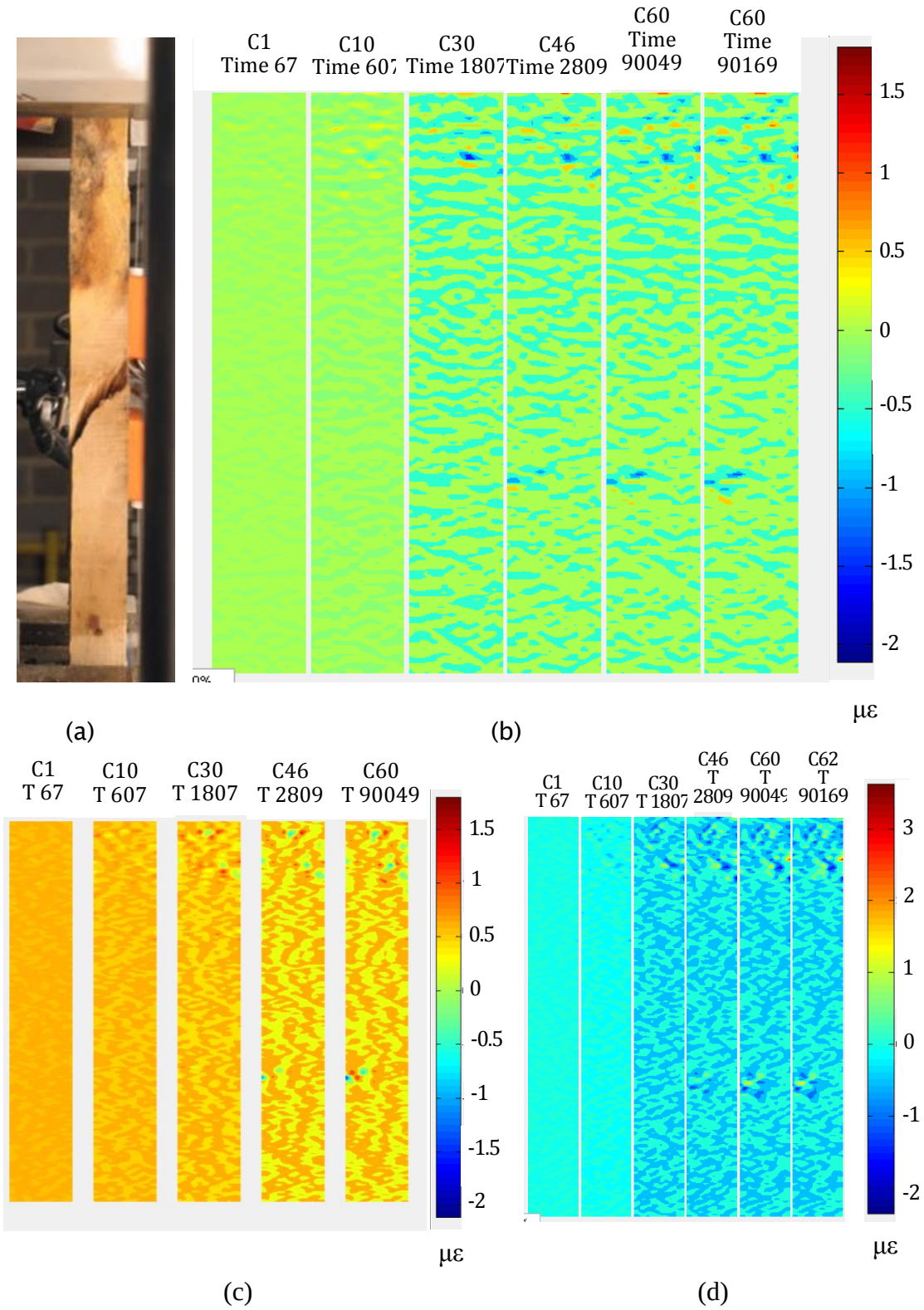

Fig. 9. (a) Failure of Sample G1S. Contour plots from sequential analysis: (b) ε_y, (c) ε_x and (d) τ_{xy}

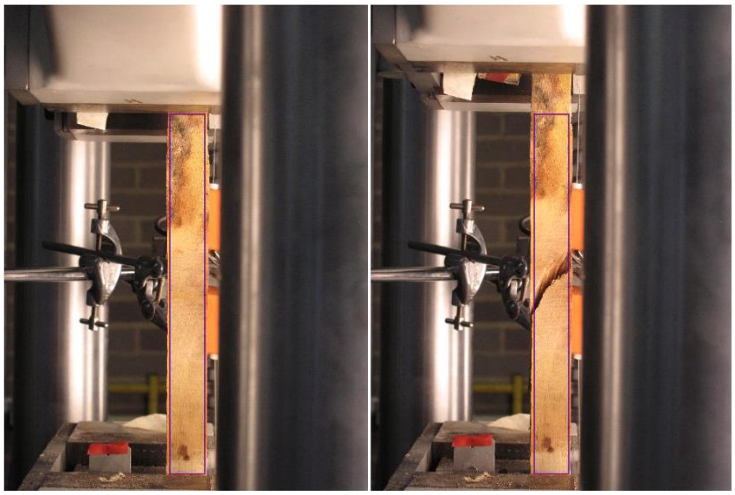

(a) (b)

Fig. 10. (a) ‘Before’ and (b) ‘After’ images of Sample G1S, with Active Area outlined

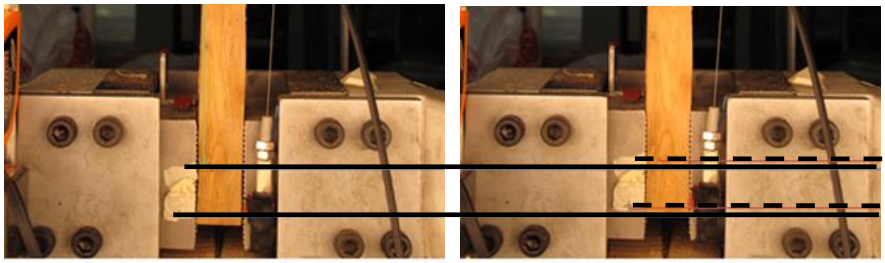

(a) (b)

Fig. 11. Movements of Fixed Point on bottom grips for Sample G1F, indicated by solid lines, (a) ‘Before’ and dashed lines (b) ‘After’

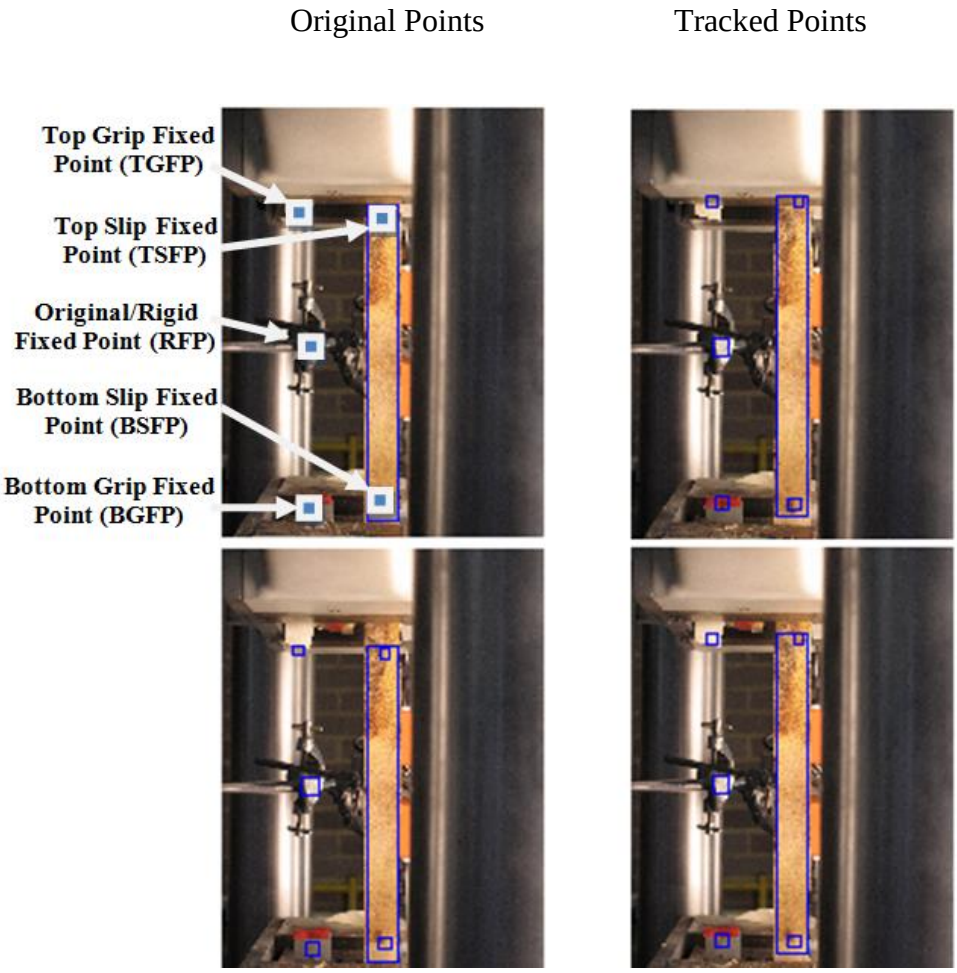

Fig. 12. Tracking Fixed Points and Active Area of sample G1S from (a) start of test to (b) pre-failure load

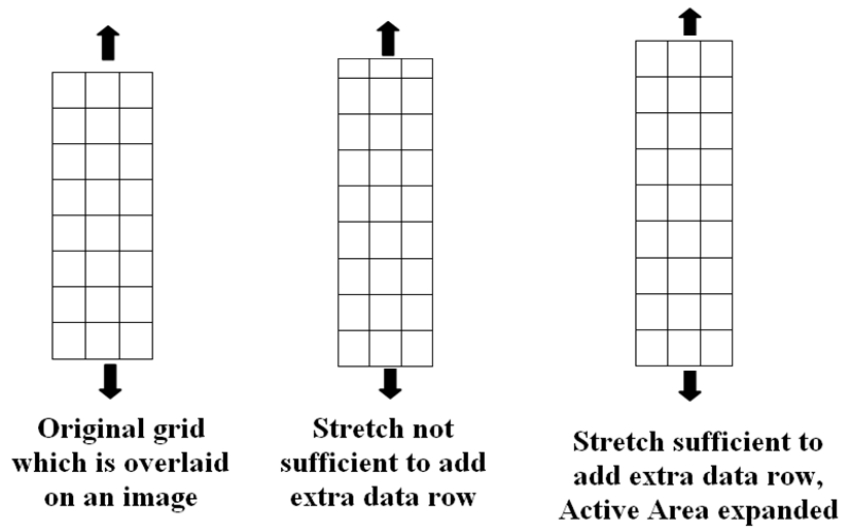

Fig. 13. Active Area grid expansion in response to sample stretch

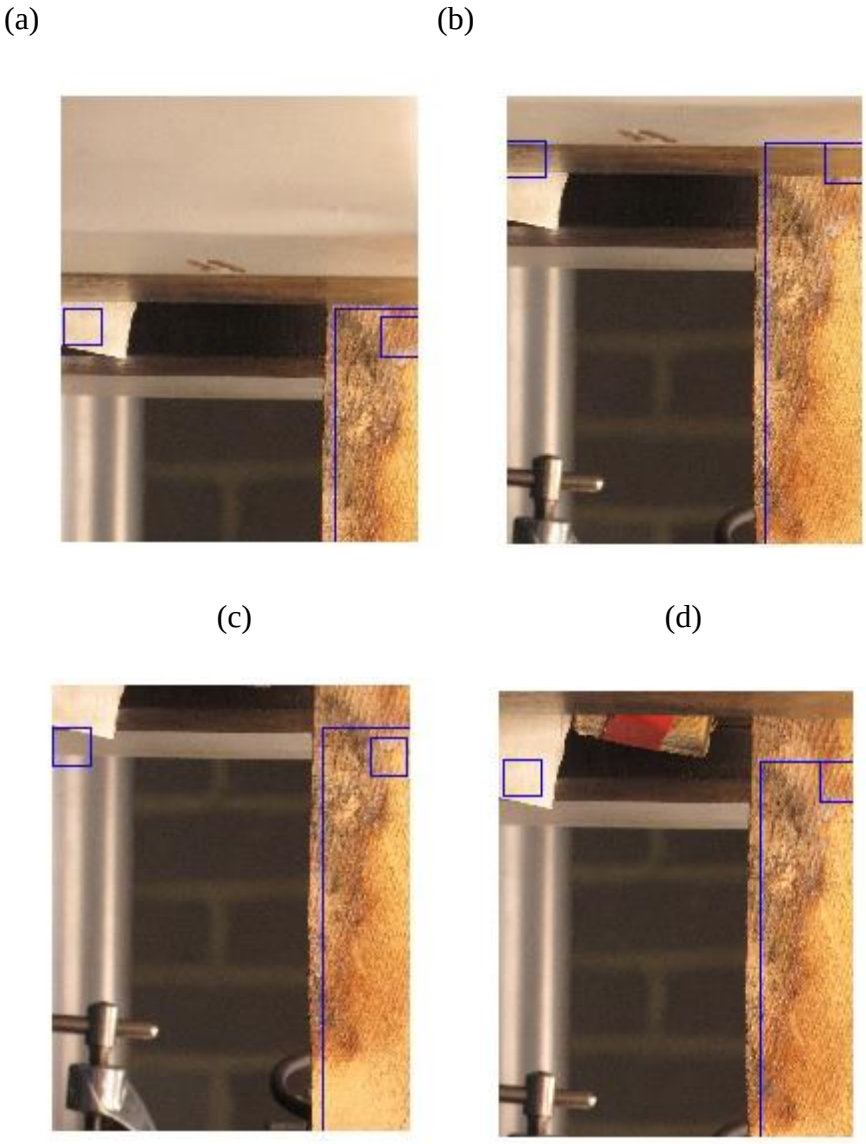

Fig. 14. Fixed Points TGFP and TSFP (squares from left to right); (a) original points, first image; (b) tracked points, first image; (c) original points, final image; (d) tracked points, final image, Sample G1S

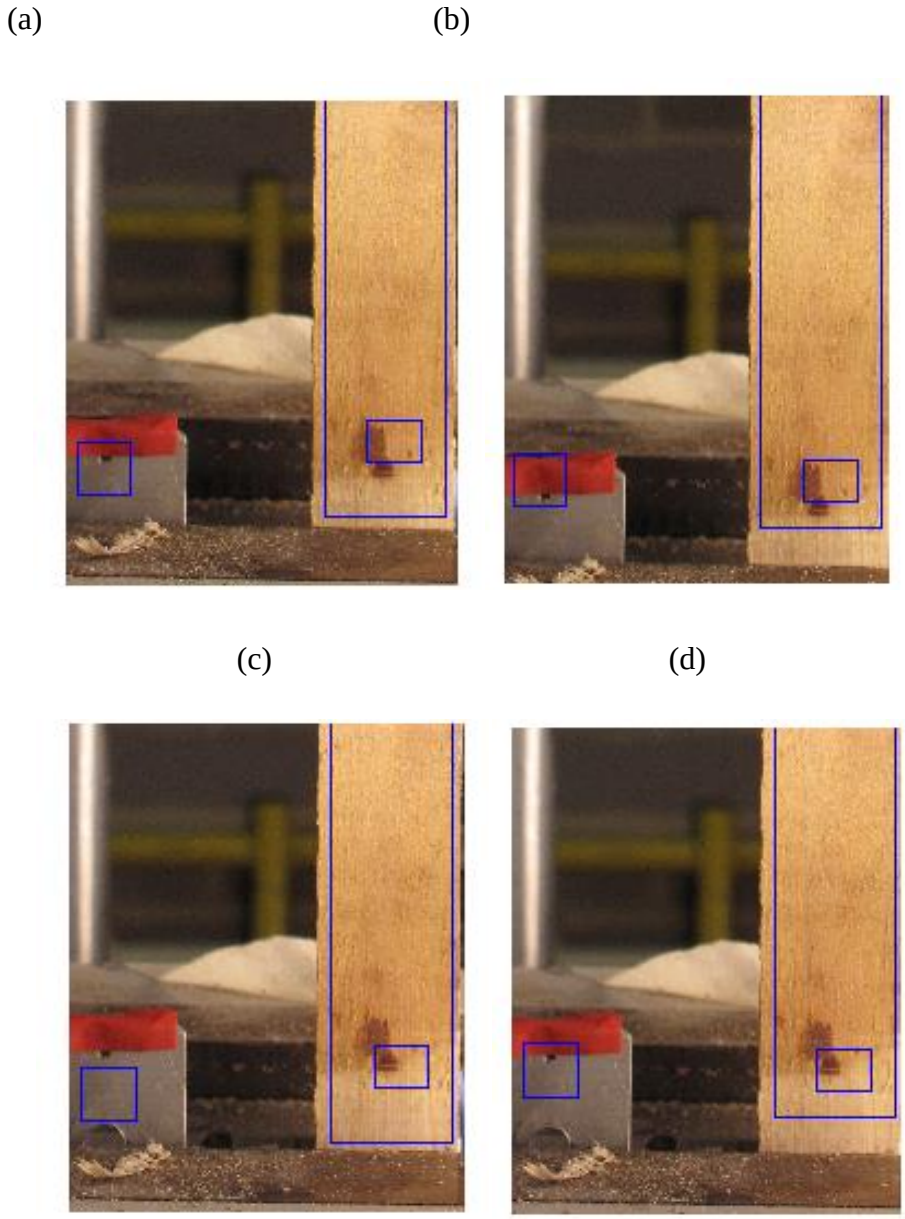

Fig. 15. Fixed Points BGFP and BSFP (squares from left to right); (a) original points, first image; (b) tracked points, first image; (c) original points, final image; (d) tracked points, final image, Sample G1S

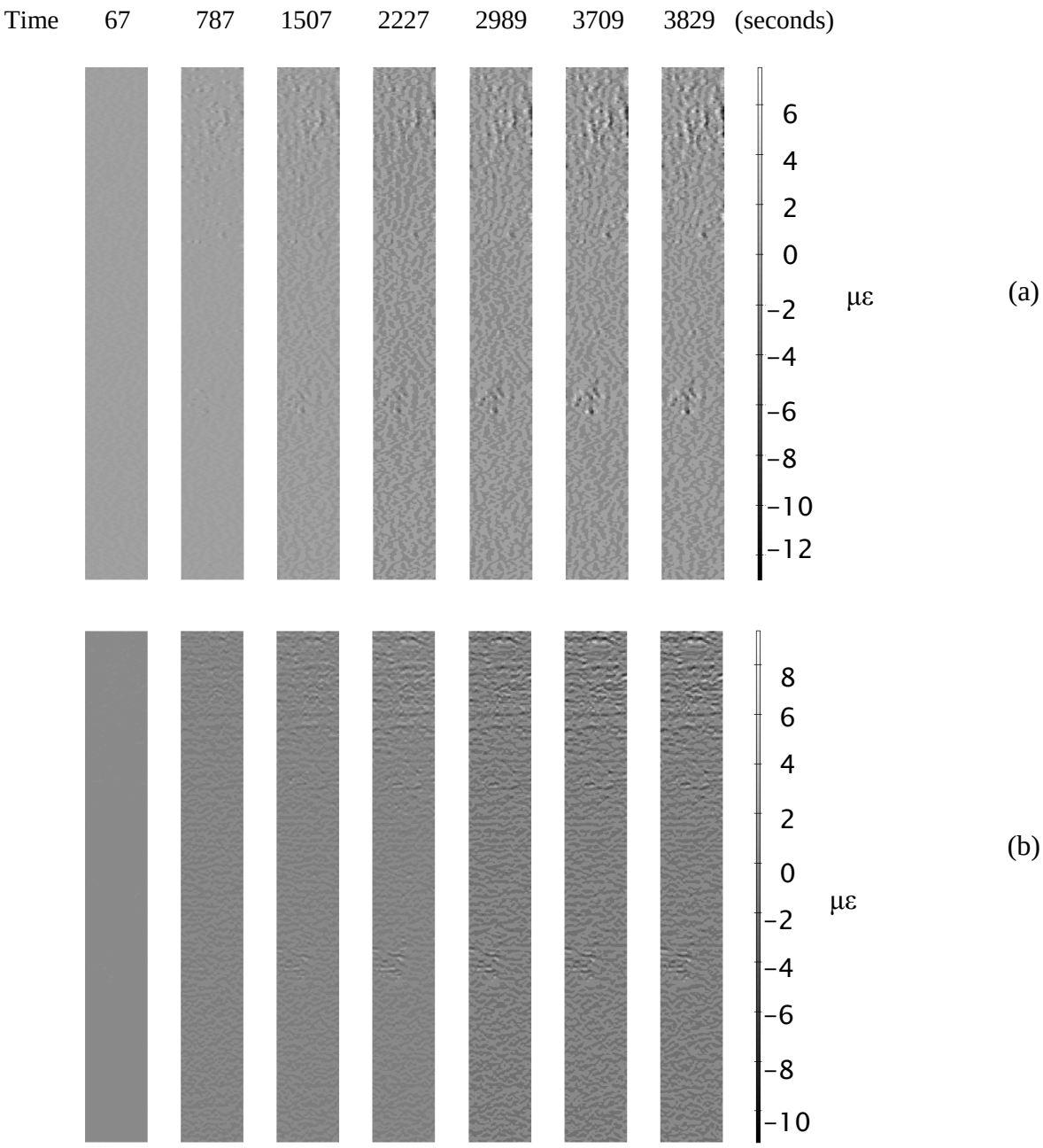
Time
67
787
1507
2227
2989
3709
3829
(seconds)
6
4
2
0
−2
−4
−6
−8
−10
−12
με
(a)
8
6
4
2
0
−2
−4
−6
−8
−10
με
(b)

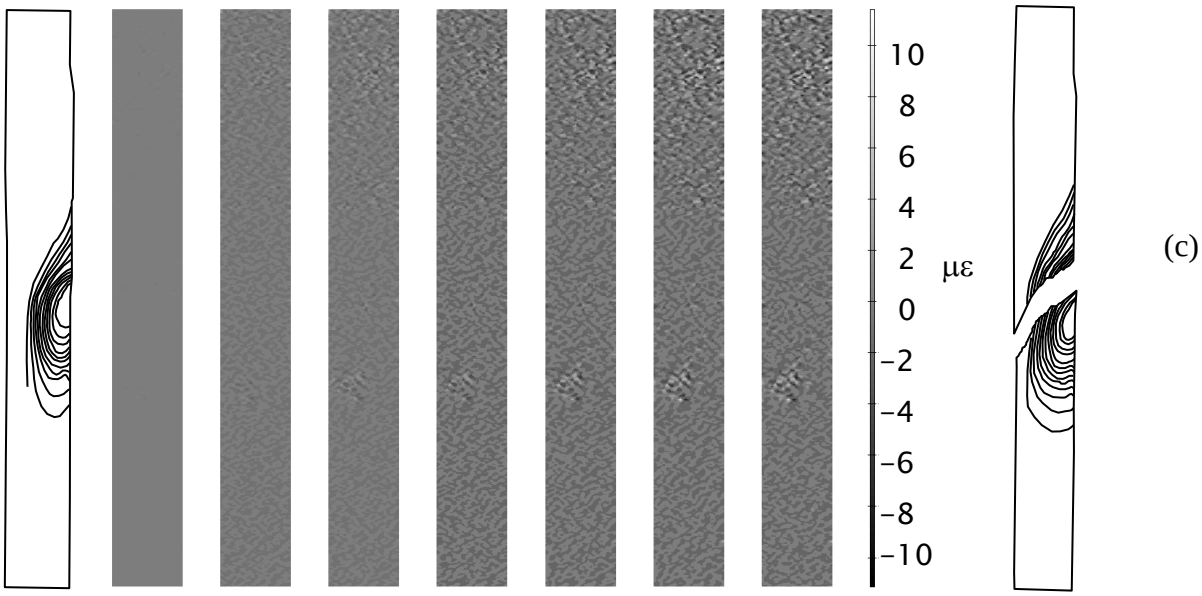

Fig. 16. Sample G1S strains from sequential analysis including Active Area tracking: (a) ε_x, (b) ε_y and (c) τ_{xy}, with grain sketches of original and failed sample

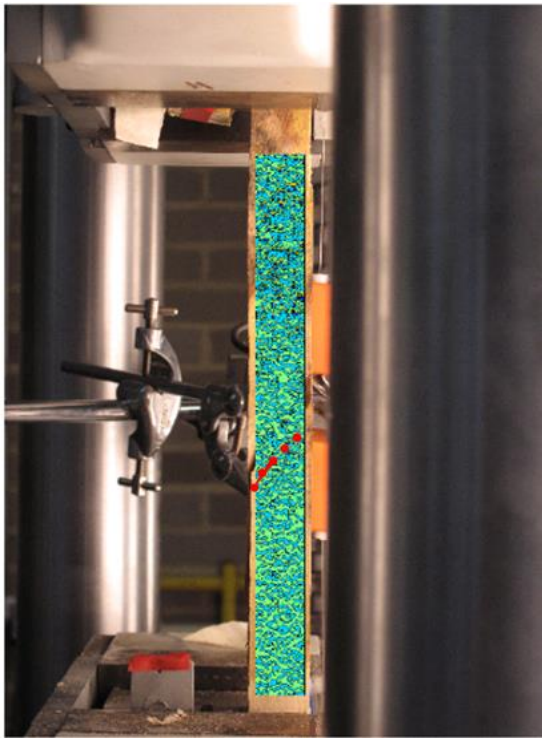

Fig. 17. Strain ε_y for Sample G1S first-last analysis (including Active Area tracking) overlaid on failure image

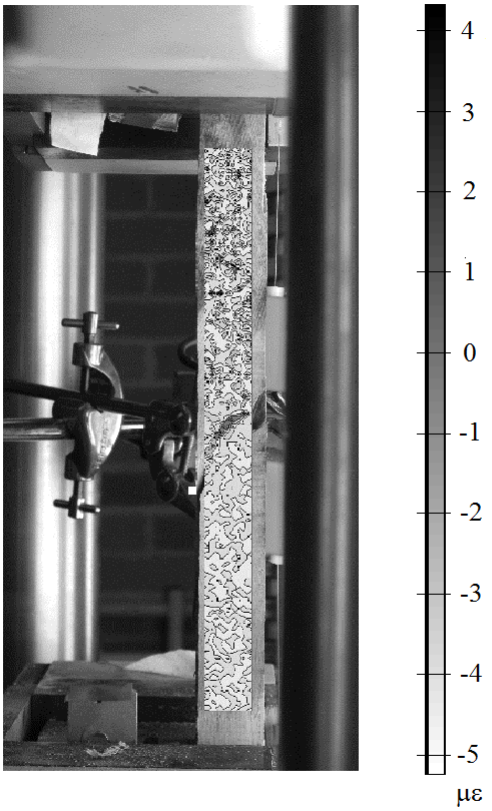

Fig. 18. True strains $(\tau_{xy})_{true}$ from first-sequential analysis of Sample G1S, overlaid on failure image

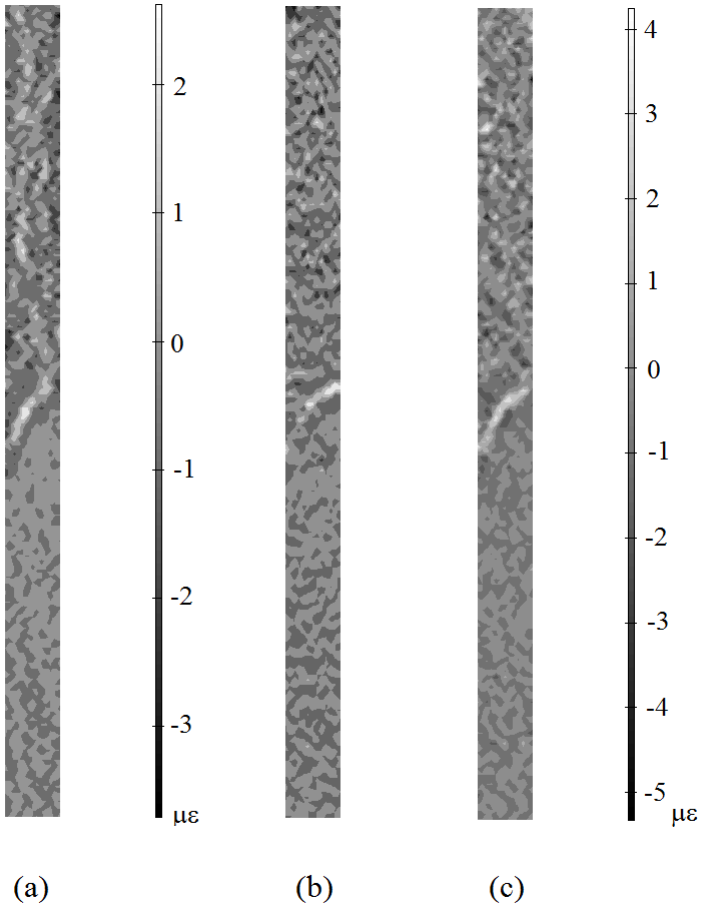

Fig. 19. Sample G1S first-sequential analysis strains: (a) ε_x, (b) ε_y and (c) τ_{xy}

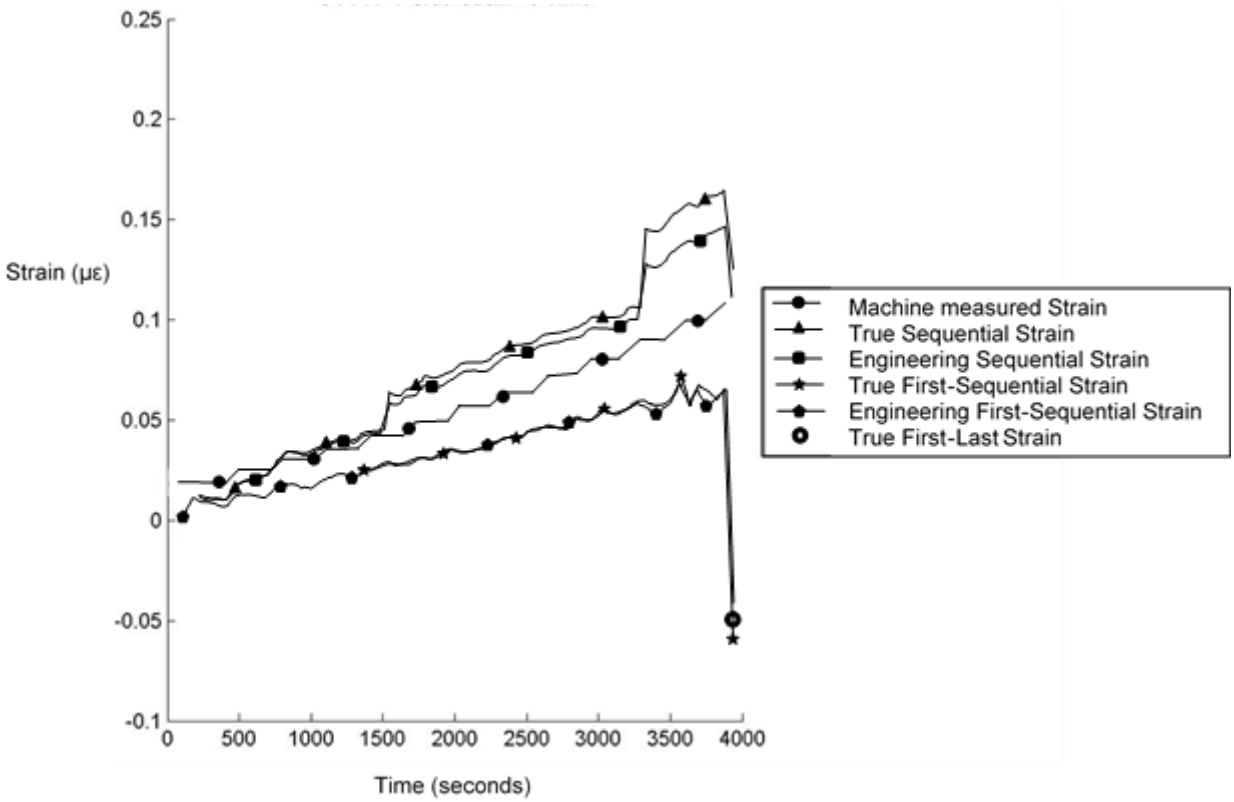

Fig. 20. Sample G1S strain ε_y against time for different PIV analysis methodologies including Active Area tracking, compared with machine measured